suggested by Schmitt and Leachman[7] in the investigation of W values for fission fragments would appear to be not appropriate. These authors have idealized the variation of W with energy by assuming it to be infinite below a certain threshold energy. The energies of the recoils used in the present experiment lie below the threshold energies found by Schmitt and Leachman, but the W values shown in Table I are only a few times larger than the alpha-particle W values. However, the trend seems to be toward larger values of W as the energy decreases.

[7] H. W. Schmitt and R. B. Leachman, Phys. Rev. **103**, 183 (1956).

The particle recoiling from the decay of ThC (Pb^{212}) is Tl^{208} having an initial velocity equal to that of an electron with about $\frac{1}{3}$ ev of energy. Obviously it cannot "knock" an electron out of an orbit, so the ionization observed must result from some other mechanism such as charge exchange.

ACKNOWLEDGMENTS

The authors wish to express appreciation to Roland Abele of the Instrument Department for his work in the design of the proportional counters, and to R. H. Ritchie for his advice and assistance in calculations.

PHYSICAL REVIEW VOLUME 107, NUMBER 3 AUGUST 1, 1957

Measurements of Large-Angle Single Collisions between Helium, Neon, and Argon Atoms at Energies to 100 kev*

E. N. Fuls, P. R. Jones, F. P. Ziemba, and E. Everhart
Physics Department, University of Connecticut, Storrs, Connecticut

(Received January 30, 1957)

Single collisions between ions and atoms have been studied at 25, 50, and 100 kev energies for the cases He^+ on He, He^+ on Ne, He^+ on A, Ne^+ on Ne, Ne^+ on A, and A^+ on A. The incident ion beam traversed a collision chamber containing a target gas whose pressure was maintained low enough to insure single interactions. The particles, which were scattered at each angle from four to forty degrees, passed through a pair of collimating holes with a resolution width of one degree. An electrostatic analyzer and its associated detectors determined the number of scattered atoms in each state of charge, ranging from zero to seven times ionized. The percentages of the various charge states in the scattered beam are plotted in order to indicate the dependence of this quantity on scattering angle and energy for each of the systems studied. The differential cross section for the scattering of particles has also been measured in each case and compared with values calculated classically from a Coulomb potential energy function modified by exponential screening.

1. INTRODUCTION

IT has been shown in previous studies[1–3] of single collisions between atoms at kev energies that the collision products resulting from such interactions are highly ionized. The recent paper[1] by two of the present authors, hereinafter called I, has described large-angle single collisions between argon ions and argon atoms at kev energies and has presented ionization and cross section data for angles out to twenty degrees. In the present paper this work has been extended. Collisions of the type He^+ on He, He^+ on Ne, He^+ on A, Ne^+ on Ne, Ne^+ on A, and A^+ on A, have been studied over an energy range of 25 to 100 kev, and measurements of the differential cross sections and distribution of charge states of the scattered particles are presented over an angular range of four to forty degrees with a resolution of ± 0.5 degree.

In addition to the papers mentioned above and the references cited therein, a paper by Kaminker and Fedorenko[4] has appeared describing the scattering of argon ions in noble gas targets at energies of 40 to 150 kev with an angular range of 0 to 15 degrees. Processes of the type $A^+ \rightarrow A^0$, $A^+ \rightarrow A^{4+}$, etc., were studied and cross sections computed for each case. It was possible in two instances to compare the measurements of Kaminker and Fedorenko with those presented in this paper, and graphs of comparable data are included in the last section.

2. EXPERIMENTAL ARRANGEMENT AND PROCEDURE

a. Apparatus

The scattering apparatus shown in Fig. 1 is nearly the same as that described previously in I. The incident ion beam enters the target gas chamber through hole *a*, and a few of the large angle collisions which happen to occur near *b* result in scattered particles which pass through resolution holes *c* and *d*. These are analyzed into their several charge states and are then detected

* This work was sponsored by the Office of Ordnance Research, U. S. Army, through the Ordnance Materials Research Office at Watertown and the Springfield Ordnance District.

[1] Carbone, Fuls, and Everhart, Phys. Rev. **102**, 1524 (1956).
[2] Everhart, Carbone, and Stone, Phys. Rev. **98**, 1045 (1955).
[3] N. V. Fedorenko, Zhur. Tekh. Fiz. **24**, 784 (1954).
[4] D. M. Kaminker and N. V. Fedorenko, Zhur. Tekh. Fiz. **25**, 2239 (1955).

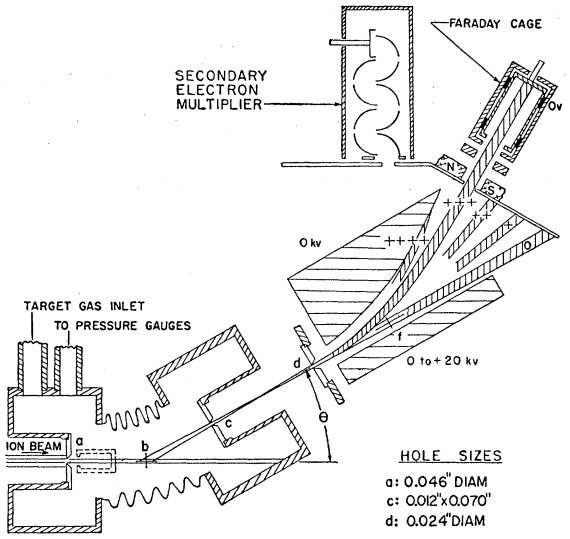

FIG. 1. The scattering apparatus.

with the Faraday cage or the secondary electron multiplier. The target gas pressure in the chamber is about one micron of mercury, which is low enough so that almost all the detected particles result from single collisions as demonstrated in I.

A change in the apparatus is the addition of a small collector cage placed directly behind hole *a* as indicated by the dotted lines. This acted as a monitor on the incident ion beam, as it could be moved into or out of the path of the beam as desired, thus providing a direct measurement of the incident ion beam inside the scattering chamber.

Increased sensitivity in the detection of small particle currents was obtained in replacing the secondary electron multiplier previously used in I. The multiplier now used is a ten-stage Dumont 6292 type with the photosensitive surface and glass envelope removed. This unit and its associated electrometer circuit permit detection of currents as low as fifty particles per second.

b. Analysis of the Scattered Particles

The data obtained at each scattering angle θ were used to determine the fraction P_n of the scattered incident particles in each charge state n. This fraction is determined from the readings of the Faraday cage detector and the secondary electron multiplier as described in I. A difficulty with the neutral component P_0 was encountered and will be more fully discussed in part d of this section. Increased accuracy and the extension of the data to larger scattering angles than in I is almost entirely due to the hundred-fold increased sensitivity of the secondary electron multiplier.

Immediately after each data set was taken, the target gas supply was cut off and the experiment repeated to to determine the scattering due to the presence of

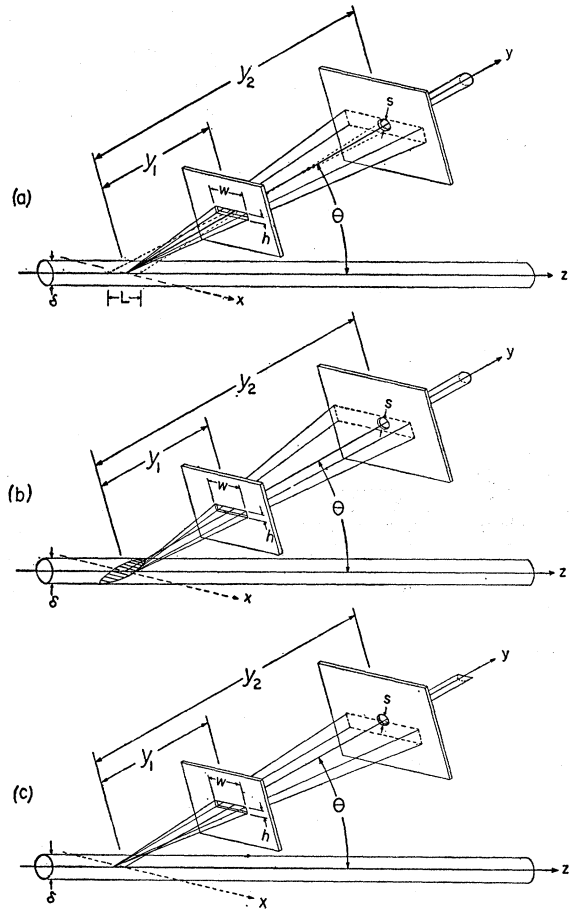

FIG. 2. (a) The scattering geometry showing the solid angle subtended by a point in the center of the target volume. (b), (c) The solid angle subtended from certain other points within the target volume.

residual gas target atoms. The pressure in the target gas chamber was then about 10^{-5} mm Hg, this being the pressure in the accelerator proper to which this chamber was connected. Since the target gas pressure was ordinarily 100 times as large, the scattered currents from the residual gas were usually negligible. However, in the case of He^+ on He collisions the cross sections to be measured are very small, and the residual gas atoms, though few in number, are of gases other than helium and individually have much larger cross sections. These currents scattered from the residual gas were subtracted from those obtained at the same angle when the target gas was present. The correction, though small in the case of collisions between heavier atoms, reached 20% in some cases of collisions of He^+ on He.

c. Differential Cross Section

The particle differential cross section is the area of the scattering center for scattering of particles irrespective of their charge after scattering, into a unit solid angle at the angle in question. This is found from the

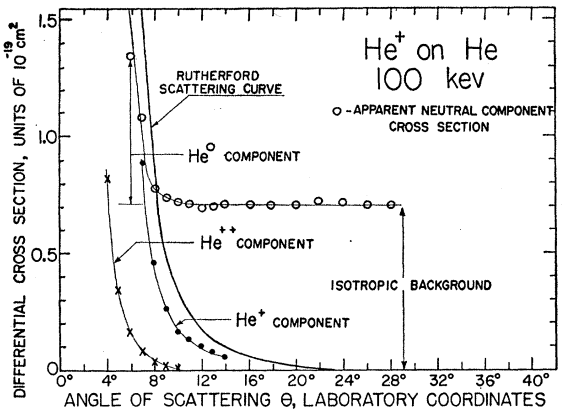

FIG. 3. The apparent differential cross section measured for the neutral component scattered from collisions of He^+ on He at 100 kev is plotted *vs* scattering angle. The isotropic background, which has been attributed to photons, is shown, and the excess above this background has been taken as the He^0 cross section. Cross-section curves are also given for the He^+ and the He^{++} components as well as the Rutherford cross section curve for comparison.

data through the expression

$$I'=N'n\sigma(\theta)L\Delta\Omega, \tag{1}$$

where I' is the number of scattered particles per second of all charge states detected at the angle θ, N' is the number of incident particles per second, n is the number of target particles per unit volume, $\sigma(\theta)$ is the particle differential cross section at that angle averaged over the effective solid angle of acceptance $\Delta\Omega$, and L is the length of the target volume in the direction of the incident ion beam. The scattering geometry is shown in Fig. 2(a) from which the length L is calculated to be

$$L=\csc\theta(y_2h+y_1s)/(y_2-y_1), \tag{2}$$

where y_1 and y_2 are the respective distances between the center of the scattering region and the collimating holes, h is the height of the rectangular first hole, and s is the diameter of the circular second hole. Here $y_1=0.916$ in., $y_2=2.228$ in., $h=0.012$ in., $s=0.024$ in., the width w of the rectangular hole is 0.070 in., and the diameter δ of the incident beam is 0.046 in. Figure 2 is drawn with h, w, s, and δ to scale with each other, but oversize in comparison with y_1 and y_2. The extreme angular width of acceptance is ± 0.8 degree, although most of the scattering comes from a more narrow angular range, about ± 0.5 degree.

These particular hole shapes have the advantage that the lateral distribution of the incident particles across the beam need not be known or assumed, since it does not enter into the calculation of the effective solid angle. A y-axis through the center of the holes and an

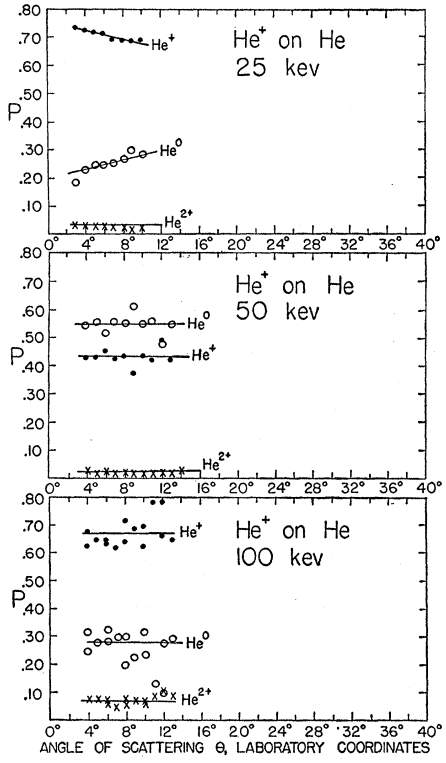

FIG. 4. The charge analysis for single collisions of He^+ on He at 25, 50, and 100 kev. Percentages in each charge state are plotted *vs* scattering angle. Empirical lines are drawn through the data.

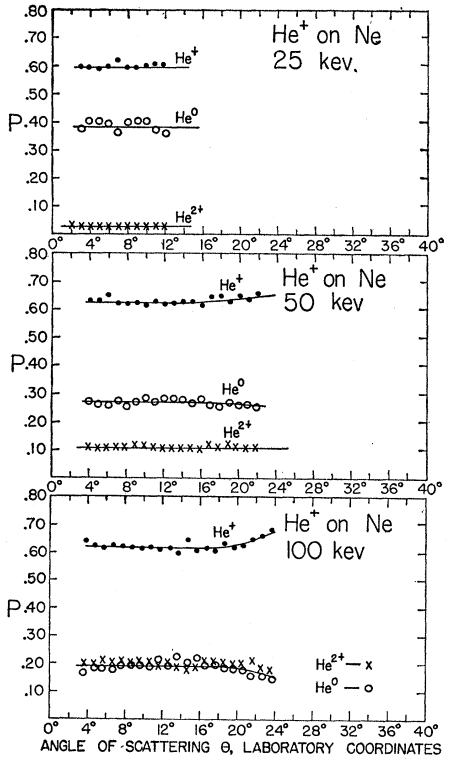

FIG. 5. The change analysis for single collisions of He^+ on Ne at 25, 50, and 100 kev. Percentages in each charge state are plotted *vs* scattering angle. Empirical lines are drawn through the data.

x-axis perpendicular to it and to the axis of the incident beam are chosen as in Fig. 2(b). It is evident that the solid angle seen from any point in the shaded area of the x, y plane is very nearly independent of the position of the point within this area. Figure 2(c) shows that the solid angle does, however, depend on the position of the point along the axis of the incident beam. The integration over the target volume yields

$$\Delta\Omega = \pi s^2 h/[4y_2(y_1 s + y_2 h)], \quad (3)$$

for the average solid angle. Equations (1)–(3) are combined to obtain a formula for the differential cross section:

$$\sigma(\theta) = 4I' y_2(y_2 - y_1)\sin\theta/(N' n \pi s^2 h), \quad (4)$$

in which all quantities can be measured.

The absolute values of the measured differential cross sections are more accurate than those reported in I because of the better scattering geometry described above and the monitor collecting cage which directly measures N' inside the target gas chamber.

d. Neutral Component

In obtaining the data, it was observed that a background, which we attributed to photons, was present with the neutral component of the scattered particles. Photons of energy between several electron volts and several hundred electron volts may be expected to result from the same violent collisions which produce the highly ionized particles. These photons upon reaching the first dynode of the electron multiplier detector could give rise to secondary electrons which would add to those produced by the neutral particles.

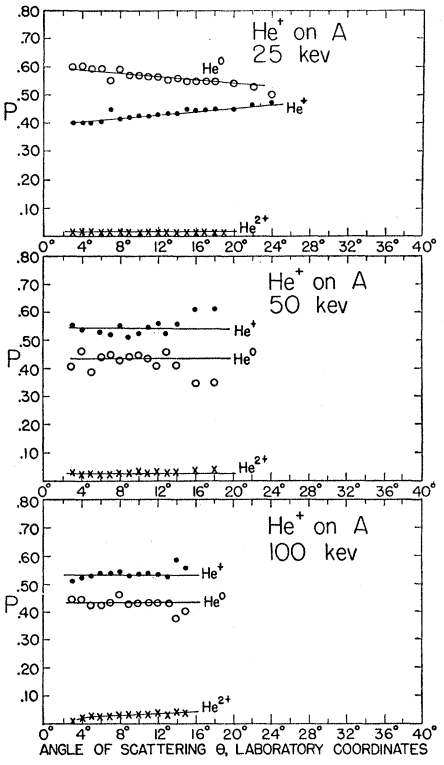

FIG. 6. The charge analysis for single collisions of He^+ on A at 25, 50, and 100 kev. Percentages in each charge state are plotted *vs* scattering angle. Empirical lines are drawn through the data.

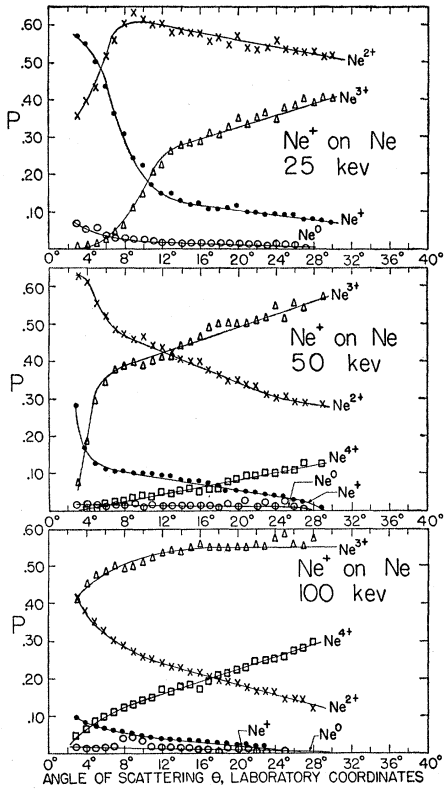

FIG. 7. The charge analysis for single collisions of Ne^+ on Neat 25, 50, and 100 kev. Percentages in each charge state are plotted *vs* scattering angle. Empirical lines are drawn through the data.

The effect of the background is shown in Fig. 3 which plots the apparent differential cross section for the scattered neutral component for collisions of He^+ on He at 100 kev *vs* angle. This quantity approaches a constant value at large angles which is hundreds of times larger than the cross sections for the charged components also shown on the diagram. In addition, it is far larger than the Rutherford scattering cross section shown in the heavy solid line. Since in this case the sum of the several components should approximate the Rutherford differential cross section,[1] it is extremely unlikely that the constant portion of the neutral cross section is due to particles.

In order to test for photons directly, a polished lithium fluoride window 1.0 mm thick was placed in the path of the neutral component in an experiment when scattering Ne^+ on Ne at various energies. Such a window would stop all particles, but would transmit photons of energy less than about 12 electron volts. These experiments were performed over the entire angular range

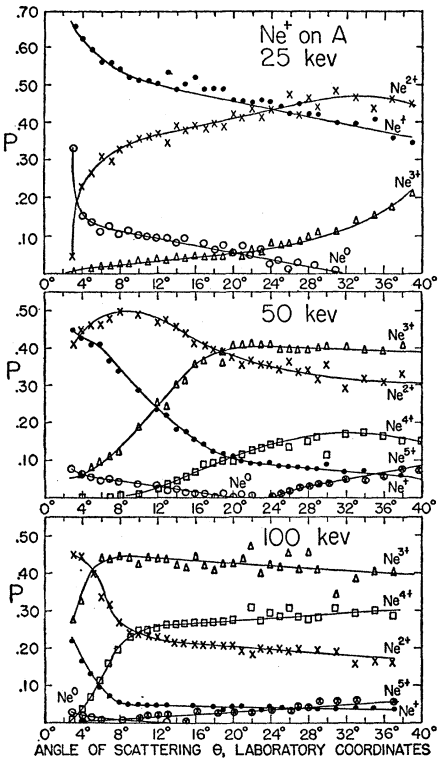

FIG. 8. The charge analysis for single collisions of Ne^+ on A at 25, 50, and 100 kev. Percentages in each charge state are plotted *vs* scattering angle. Empirical lines are drawn through the data.

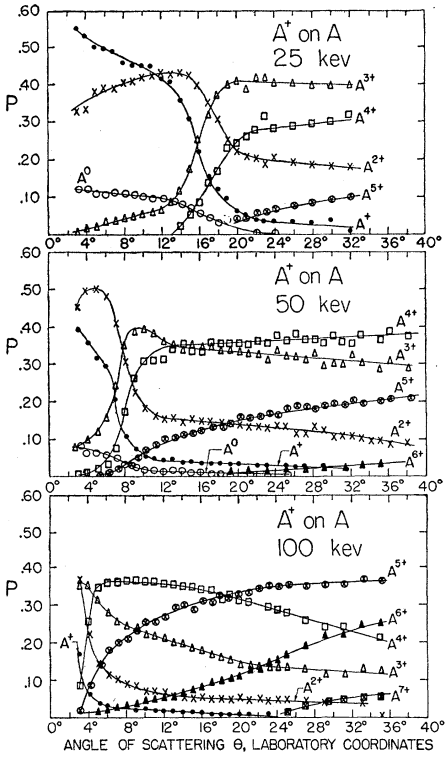

FIG. 9. The charge analysis for single collisions of A^+ on A at 25, 50, and 100 kev. Percentages in each charge state are plotted *vs* scattering angle. Empirical lines are drawn through the data.

including large angles where the apparent differential cross section for neutrals had reached a constant value. The readings on the multiplier detector indicated that photons were indeed present and that their distribution was isotropic. The readings were, however, only 5% of the readings previously attributed to photons in the corresponding experiment without the window. The most reasonable interpretation is that most of the photons were too energetic to pass through this window.

In the data to be presented in the next section, the isotropic portion of the neutral component was subtracted in all cases to obtain the readings for the neutral particles alone. It should not be inferred that the cross section for creating photons has the absolute value shown in Fig. 3 for that particular case, since the multiplicative factor which converts the output of the electron multiplier detector to the input particle current is not necessarily the same for photons as for helium particles.

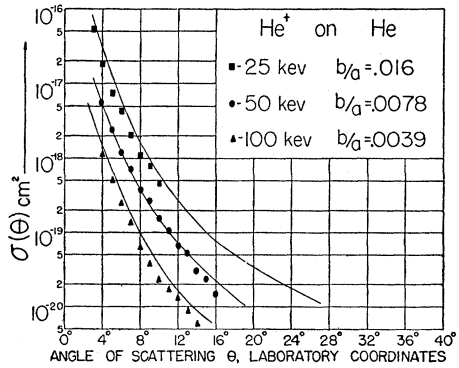

FIG. 10. Particle differential cross sections for single collisions of He^+ on He at 25, 50, and 100 kev plotted *vs* scattering angle. The solid lines show computed cross sections.

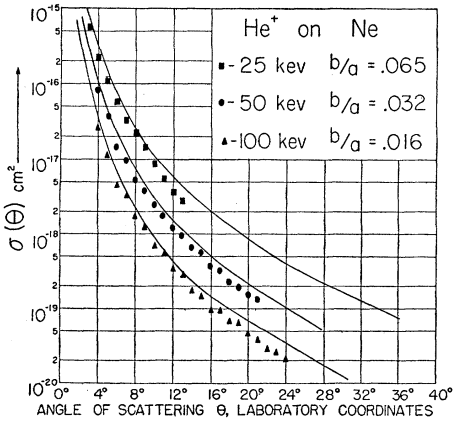

FIG. 11. Particle differential cross sections for single collisions of He^+ on Ne at 25, 50, and 100 kev plotted *vs* scattering angle. The solid lines show computed cross sections.

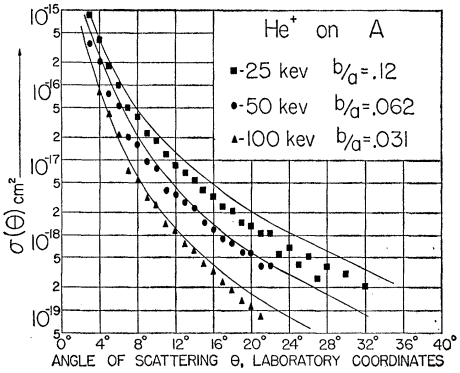

FIG. 12. Particle differential cross sections for single collisions of He^+ on A at 25, 50, and 100 kev plotted *vs* scattering angle. The solid lines show computed cross sections.

Unfortunately, this difficulty with photons limited the angular extent to which the data could be plotted, particularly in those cases where helium ions were the incident particles. For these interactions a major portion of the scattered particles were neutral, and the analysis became uncertain as soon as the photon component became considerably larger than the neutral particle component. In the case of collisions of Ne^+ on Ne, Ne^+ on A, and A^+ on A, the neutral particle component became negligible with increasing angle compared to the charged components, and the data could, therefore, be carried out to fairly large angles.

3. DATA AND DISCUSSION

a. Charge Analysis

The charge analyses of the scattered incident particles from collisions of He^+ on He, He^+ on Ne, He^+ on A, Ne^+ on Ne, Ne^+ on A, and A^+ on A at energies of 25, 50, and 100 kev are shown in Figs. 4 through 9, respectively. The fractions P_n in each charge state are plotted against angle θ in the laboratory coordinate system.

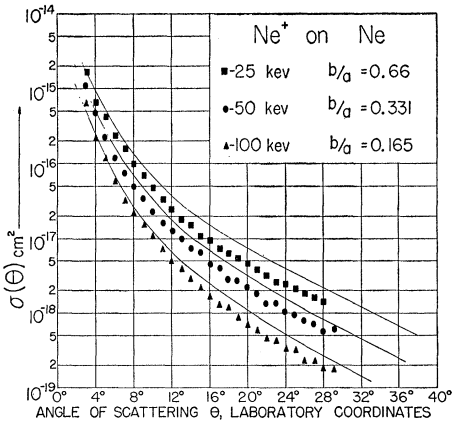

FIG. 13. Particle differential cross sections for single collisions of Ne^+ on Ne at 25, 50, and 100 kev plotted *vs* scattering angle. The solid lines show computed cross sections.

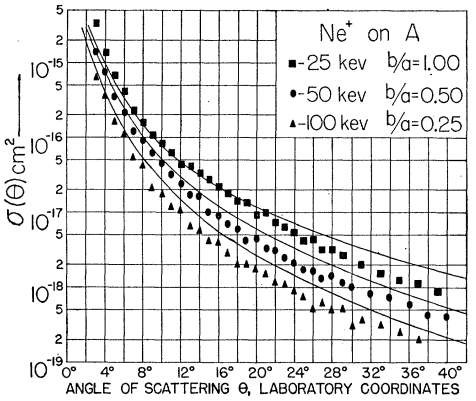

FIG. 14. Particle differential cross sections for single collisions of Ne^+ on A at 25, 50, and 100 kev plotted *vs* scattering angle. The solid lines show computed cross sections.

Each graph contains two independent data sets obtained on different days, one taken at odd angles and the other at even angles.

Figures 4, 5, and 6 show that the analysis of the scattered helium particles does not depend significantly on angle, although it does depend on energy and the kind of target gas. The data in Figs. 7, 8, and 9, wherein neon and argon ions are incident, do show a strong dependence on angle and incident ion energy. It is observed generally that more energetic collisions result in more highly ionized products, and at large angles the particles are more highly ionized on the average than at small angles. In comparing the Ne^+ on A data of Fig. 8 with the A^+ on A data of Fig. 9, it is seen that the scattered argon particles are more highly ionized than the scattered neon particles at comparable energies and angles.

Collisions of A^+ on A were also discussed in I and from those data it appeared that the fractions P_n were a function of distance of closest approach alone. This conclusion is not supported by the present data of

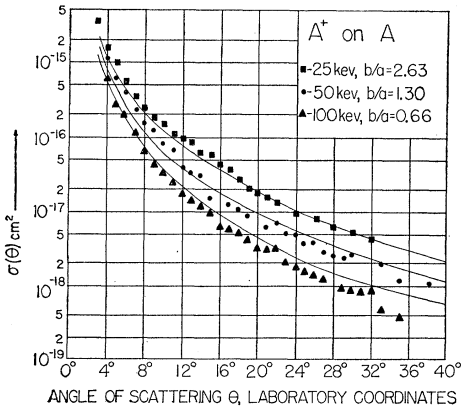

FIG. 15. Particle differential cross sections for single collisions of A^+ on A at 25, 50, and 100 kev plotted *vs* scattering angle. The solid lines show computed cross sections.

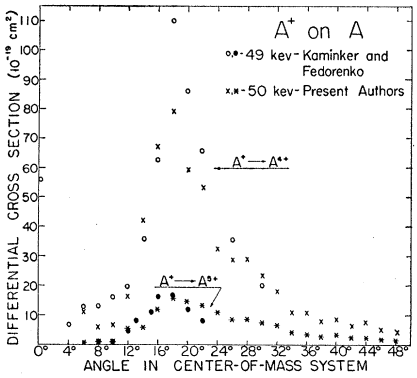

FIG. 16. A comparison of the data of this paper with those of Kaminker and Fedorenko. Differential cross sections at 49 and 50 kev for the process $A^+ \rightarrow A^{4+}$ and $A^+ \rightarrow A^{5+}$ with argon targets are plotted *vs* angle in the center-of-mass system.

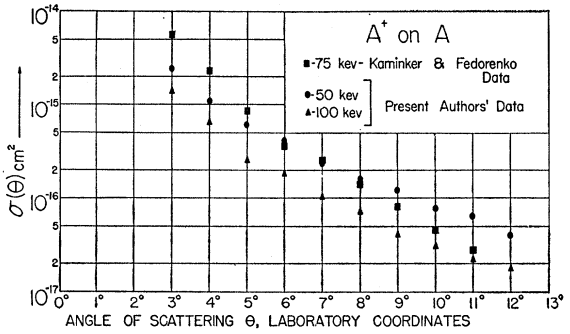

FIG. 17. The particle differential cross section for the scattering of A^+ on A is plotted *vs* angle in the laboratory system. The 50- and 100-kev data are from this paper and the 75-kev data are from the work of Kaminker and Fedorenko.

Figs. 7, 8, and 9. When these new data were plotted as a function of distance of closest approach, as in Figs. 6 and 7 of I, it was found that there was also an energy dependence which had been masked in the less accurate earlier data.

b. Differential Cross Sections

The measurements of the particle differential cross sections $\sigma(\theta)$ in square centimeters for all the collisions studied are shown in Figs. 10 through 15. The points for each energy represent two independent data sets, and are computed from the data using Eq. (4).

The solid lines appearing in each figure are cross sections computed classically[5] from a screened Coulomb potential energy function in terms of a parameter b/a which depends only on the energy of the collision and the constants of the atoms involved. This calculation is discussed more fully in I, and that paper reported a favorable comparison of theory and experiment in the case of collisions of A^+ on A. The present comparison confirms this result, showing good agreement in all cases studied. At large angles, most of the measured points consistently fall below the computed curves. This suggests that the potential energy function used in the calculations may not precisely describe the actual interaction.

The He^+ on He cross-section data of Fig. 10 are particularly important in that the screening effect is negligible and the scattering can be computed quite accurately using the familiar Rutherford scattering formula. The excellent agreement in absolute magnitude between the data and the computed curves in this case indicates that there is no excessive systematic error in the measurement.

It was also possible to compare some of the results presented here with those given in the paper by Kaminker and Fedorenko.[4] In one case they present 49-kev measurements of the differential cross sections for the processes $A^+ \rightarrow A^{4+}$ and $A^+ \rightarrow A^{5+}$ (with argon targets) as functions of the angle in the center-of-mass system. By combining the cross sections measured at 50 kev for the A^+ on A curves of Fig. 15 with the analysis of Fig. 9, comparable cross sections can be obtained from our data, and converted to center-of-mass coordinates. Our data are compared in Fig. 16 with that of Kaminker and Fedorenko and show good agreement.

In one of their figures, Kaminker and Fedorenko present particle differential cross section measurements for the A^+ on A collisions at 75 kev. Their data have been converted to the laboratory coordinate system and replotted on Fig. 17 where they are compared with our data for 50 kev and 100 kev. Here there is agreement as to the magnitude of the cross sections, but some differences with respect to the slope of the curves.

In conclusion, we should like to express our appreciation to Dr. Arnold Russek for helpful discussions of the experiment.

[5] Everhart, Stone, and Carbone, Phys. Rev. **99**, 1287 (1955).